The Astrophysical Journal, 586:128–134, 2003 March 20

KECK SPECTROSCOPY AND *HUBBLE SPACE TELESCOPE* IMAGING OF GRB 000926: PROBING A HOST GALAXY AT $z = 2.038$

S. Castro,[1,2] T. J. Galama,[1] F. A. Harrison,[1] J. A. Holtzman,[3] J. S. Bloom,[1] S. G. Djorgovski,[1] and S. R. Kulkarni[1]

Received 2001 October 24; accepted 2002 November 26

ABSTRACT

We present early-time Keck spectroscopic observations and late-time *Hubble Space Telescope* (*HST*) imaging of GRB 000926. The *HST* images show a small offset between the optical transient and a bright, compact knot in the host galaxy. Combined with the large equivalent widths measured for metallic absorption lines by the Keck Echellette Spectrograph and Imager (ESI) and the Low Resolution Imaging Spectrometer, this indicates that the GRB exploded inside a region of high stellar density. The ESI spectroscopy reveals two absorption systems centered at $z = 2.0379 \pm 0.0008$ with a velocity separation of 168 km s^{-1}, which we interpret as being due to individual features in the host galaxy. The ratios of chromium to zinc equivalent widths indicate that the host is depleted in dust relative to local values to a similar degree as damped Lyα systems at the same redshift.

Subject headings: galaxies: high-redshift — gamma rays: bursts

1. INTRODUCTION

Observational evidence indicates that gamma-ray bursts (GRBs) explode in luminous regions of galaxies, implying that the progenitors of these events have a distribution similar to galactic stellar components. *Hubble Space Telescope* (*HST*) imaging reveals that GRB optical transients (OTs) have smaller offsets relative to the centers of their host galaxies than would be expected for a halo population (Bloom, Djorgovski, & Kulkarni 2001). A few events have exhibited large optical extinctions, such that they are visible only at X-ray, IR, and radio wavelengths (Groot et al. 1997; Taylor et al. 1998; Djorgovski et al. 2001). This indicates these exploded in or behind dense regions of the host galaxy. The large equivalent widths (EWs) of metallic absorption lines seen in spectra of GRB OTs also point to a dense location. This location of GRBs within their hosts is consistent with popular progenitor models that suggest that GRBs may descend from massive stars (MacFadyen & Woosley 1999).

If GRBs are associated with a young stellar population, a typical line of sight toward an event will intersect a significant column of the galactic interstellar medium (ISM). Intermediate- and high-resolution absorption spectroscopy can therefore be used to probe the metal content of the host as well as individual structures, if they are separated by sufficient Doppler shifts. Ratios of metal lines can also be used to probe the dust content. For example, the Zn II ($\lambda\lambda$2025, 2062) doublet is a good indicator of metallicity, since it has near-solar abundance in gas with little depletion onto interstellar grains (Pettini, Boksenberg, & Hunstead 1990). Cr, on the other hand, exists mostly in interstellar grains and is among the most heavily depleted elements in the gas phase of the ISM. Measuring both the Zn II doublet as well as the Cr II triplet ($\lambda\lambda$2055, 2061, 2065) therefore provides a qualitative measure of the dust-to-gas ratio (Pettini et al. 1990, 1994).

Comparing chemical composition and dust content in a sample of GRB host galaxies to, for example, damped Lyα systems at similar redshift would indicate whether GRBs occur in regions with unusual metal enrichment. Since it is unclear what factors, other than mass, play a role in determining which stellar progenitors produce GRBs, this could provide direct clues to the explosion. It is also interesting to look for anomalously low dust-to-gas ratios. It has been theorized that the early, hard radiation from the GRB and its afterglow should destroy dust in the circumburst environment (Perna & Loeb 1998; Waxman & Draine 2000; Fruchter, Krolik, & Rhoads 2001). The destruction of dust grains would release metals and increase the relative EWs of those elements preferentially condensed onto dust grains.

In this paper, we present early-time spectroscopic observations with the W. M. Keck telescope of the afterglow of GRB 000926 using the Echellette Spectrograph and Imager (ESI) and the Low Resolution Imaging Spectrometer (LRIS), combined with imaging of the host galaxy by *HST*.

1.1. *GRB 000926*

The Interplanetary Network (*Ulysses*, Konus/*Wind*, and *NEAR*) detected the long-duration ($t_\gamma = 25$ s) event GRB 000926 on UT 2000 September 26.993 (Hurley et al. 2000). Gorosabel et al. (2000) and Dall et al. (2000) identified the afterglow. The discovery and optical light curves are presented in Fynbo et al. (2001). Spectra of the afterglow from the Nordic Optical Telescope yielded an absorption redshift of 2.066 (Fynbo et al. 2000), later refined to 2.0379 ± 0.0008 from Keck spectroscopy (Castro et al. 2000).

Ground-based multicolor light curves of the afterglow show a steepening beginning $\sim$1.2 days after the event (Price et al. 2001), providing evidence that the ejecta are collimated into a jet. The gamma-ray energy release, corrected for the implied collimation, is 2.2×10^{51} ergs. A fit of the data to an afterglow model requires modest extinction in excess of the Galactic value along the line of sight (A_V in the range 0.11–0.82 mag; see Price et al. 2001), presumably due to the host galaxy. Synthesis of the broadband data set resulting from *Chandra* X-ray observations, continued optical monitoring by *HST*, and Very Large Array radio observations reveal

[1] Palomar Observatory, 105-24, California Institute of Technology, Pasadena, CA 91125.

[2] Infrared Processing and Analysis Center, 100-22, California Institute of Technology, Pasadena, CA 91125.

[3] Department of Astronomy, New Mexico State University, Box 30001, Department 4500, Las Cruces, NM 88003-8001.

evidence that the cooling is dominated by inverse Compton scattering, with the IC component directly observable (Harrison et al. 2001). This implies that the GRB exploded in a moderately dense, $n \sim 30\ \mathrm{cm}^{-3}$ medium, consistent with a diffuse interstellar cloud environment.

2. OBSERVATIONS

2.1. *Moderate-Resolution Spectroscopy*

The first spectrum of GRB 000926 was taken 29 hr and 17 minutes after the burst, starting at about UT 2000 September 29.26. L. Cowie obtained two spectra, each of 1800 s duration, using ESI (Epps & Miller 1998) in the echelle mode. In this mode, the spectrum covers the range 3900–10900 Å over 10 orders. We used the 1″ slit, which yields 11.4 km s^{-1} $pixel^{-1}$ for the spectral resolution of the instrument. The two spectra were obtained at an air mass of about 1.33 and position angle of 128°, about 15° from the parallactic angle.

We employed two procedures for data reduction, one using standard IRAF packages and the other using the Mauna Kea Echelle Extraction (MAKEE) program (written by T. Barlow). The two reductions agreed to within statistical errors. We reduced the echelle orders using a bright star to trace each individual order prior to extraction. Each exposure was optimally extracted and background-subtracted. We identified lines in CuAr lamp spectra, individually extracted using the object's apertures, and determined the wavelength scale by polynomial-fitting the line positions with a mean rms of 0.09 Å. The two spectra were then added to yield the final spectrum.

2.2. *Low-Resolution Spectroscopy*

Low-resolution spectra of the GRB 000926 afterglow were obtained using LRIS (Oke et al. 1995) on the Keck I telescope. R. Ellis obtained two exposures of 900 s each on UT 2000 September 29, 29 hr and 27 minutes after the burst, using the 1.″0 slit with the 600 line mm^{-1} grating, which provides a resolution of ~1,000. The two exposures were taken at slightly different positions on the slit. Data reduction followed similar procedures to those employed for ESI. The two images were then subtracted from each other so as to yield a sky-subtracted image. We used a NeAr+HgKr arc lamp to wavelength-calibrate the data.

2.3. *HST Imaging*

As part of an *HST* Cycle 9 program, we observed GRB 000926 at five epochs with the Wide Field Planetary Camera 2 (WFPC2). We reported results from the first four epochs, taken between UT 2000 October 7.25 and December 16.9, in Harrison et al. (2001). In these early epochs, emission from the OT made a significant contribution to the total measured flux from the GRB position. We observed at a fifth epoch, UT 2001 May 19.63–20.86, in the F450W, F606W, and F814W WFPC2 filters, and we present these results along with a comparison to previous epochs here.

HST was pointed such that the OT falls on WFPC CCD 3 at the WFALL position. The 2200 s (1 orbit each) F450W images were combined using the STSDAS task CRREJ. The F606W and F814W images were observed at two offsets, by +2.5, +2.5 pixels in x and y. These images were combined and cosmic-ray rejected using the DRIZZLE technique (Fruchter & Hook 2002). The drizzled images have pixels half the area of the original WFPC data.

TABLE 1

THE ESI LINE IDENTIFICATIONS WITH EQUIVALENT WIDTH MEASUREMENTS

Line	λ_{vac} (Å)	z_{abs}	$W_{\lambda,\mathrm{rest}}$ (Å)
Si IV λ1393.76.....	4234.76	2.03837	2.13 ± 0.21
Si II λ1526.72.....	4637.71	2.03769	2.64 ± 0.26
C IV λ1548.20.....	4703.33	2.03794	2.60 ± 0.26
C IV λ1550.77.....	4711.74	2.03832	2.46 ± 0.25
Fe II λ1608.46.....	4885.84	2.03759	2.15 ± 0.22
Al II λ1670.81.....	5075.48	2.03773	2.53 ± 0.25
Si II λ1808.00.....	5492.60	2.03794	1.13 ± 0.11
Al III λ1854.72.....	5634.81	2.03809	1.57 ± 0.16
Al III λ1862.78.....	5659.09	2.03798	1.27 ± 0.13
Zn II λ2026.14	6155.55	2.03806	0.90 ± 0.09
Cr II λ2056.25.....	6246.85	2.03798	0.69 ± 0.07
Cr II λ2062.23.....	6267.67	2.03927	0.23 ± 0.02
Zn II λ2062.66	6268.12	2.03885	0.05 ± 0.01
Cr II λ2066.16.....	6278.52	2.03874	$0.18 > W_{\lambda,\mathrm{rest}} > 0.09$
Fe II λ2344.21.....	7121.43	2.03788	3.41 ± 0.34
Fe II λ2374.46.....	7213.28	2.03786	2.57 ± 0.26
Fe II λ2382.76.....	7236.64	2.03708	3.07 ± 0.31
Fe II λ2600.18.....	7899.17	2.03793	3.65 ± 0.37
Mg II λ2796.35	8494.57	2.03774	5.35 ± 0.54
Mg II λ2803.53	8515.53	2.03743	5.41 ± 0.54
Mg I λ2852.97	8667.56	2.03809	2.43 ± 0.24

NOTE.—The errors indicate a 10% uncertainty due to the continuum placement.

3. METALLIC LINE ABSORPTION

Our ESI spectra show one absorption system, split into two components, identified by the lines listed in Table 1. The lower resolution LRIS spectrum does not resolve the two components but finds a single absorption system with lines listed in Table 2. The mean redshift obtained from these lines is $z = 2.0373 \pm 0.0011$ (LRIS) and $z = 2.0379 \pm 0.0008$ (ESI).

Figure 1 shows the ESI spectrum smoothed by a boxcar of 7 pixels, equivalent to 1.12 Å. The absorption lines show evidence for two components with a mean separation of ~4.05 Å (seen in Figs. 2 and 3). Table 1 shows the line

TABLE 2

THE LRIS LINE IDENTIFICATIONS

Line	λ_{vac} (Å)	z_{abs}	$W_{\lambda,\mathrm{rest}}$ (Å)
Si IV λ1393.76.....	4232.52	2.03676	$2.46 \pm 0.25\ (0.03)$
Si II λ1526.72.....	4638.35	2.03811	$3.31 \pm 0.33\ (0.01)$
C IV λ1548.20.....	4702.54	2.03742	$1.88 \pm 0.19\ (0.02)$
C IV λ1550.77.....	4711.15	2.03794	$1.91 \pm 0.19\ (0.02)$
Fe II λ1608.46.....	4886.10	2.03775	$2.57 \pm 0.26\ (0.01)$
Al II λ1670.81.....	5075.81	2.03613	$2.47 \pm 0.25\ (0.03)$
Si II λ1808.00.....	5491.96	2.03759	$1.39 \pm 0.14\ (0.02)$
Al III λ1854.72.....	5633.60	2.03744	$2.06 \pm 0.21\ (0.02)$
Al III λ1862.78.....	5655.15	2.03586	$1.95 \pm 0.19\ (0.01)$
Zn II λ2026.14	6155.67	2.03813	$1.20 \pm 0.12\ (0.01)$

NOTE.—Systematic and statistical (in parentheses) errors are indicated.

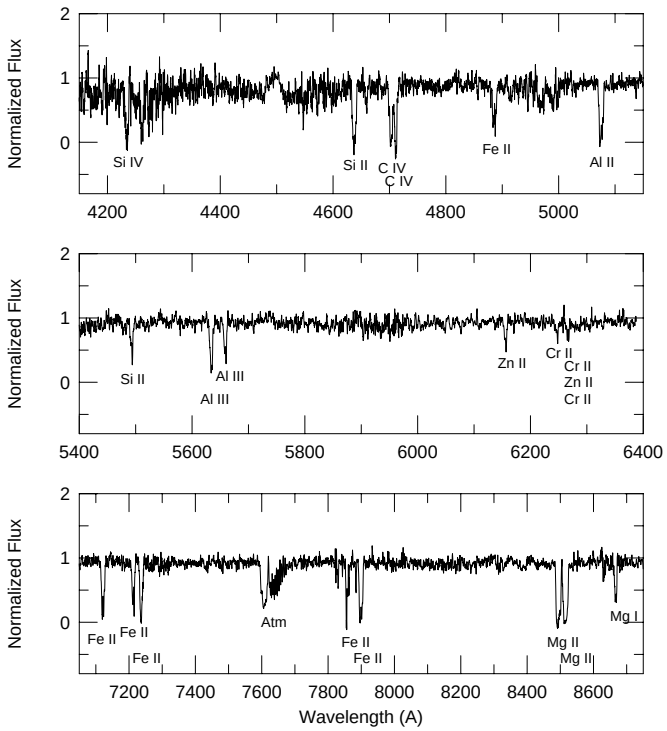

FIG. 1.—ESI spectrum of GRB 000926 on UT 2000 September 29.26. Indicated are the line identifications corresponding to a redshift of $z = 2.0372 \pm 0.0008$. The absorption feature around 7600 Å is an atmospheric line due to telluric O_2. The spectrum has been smoothed by a boxcar of 7 pixels, equivalent to 1.12 Å.

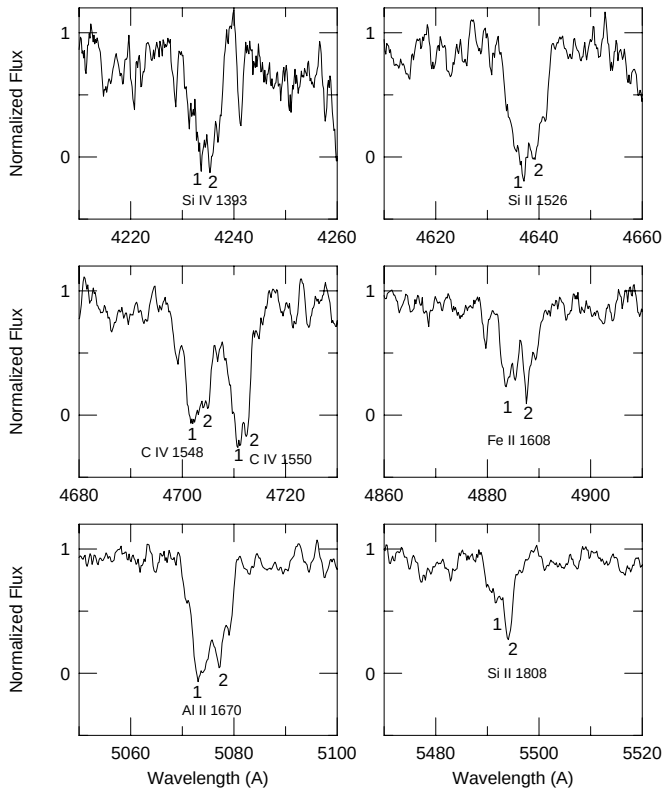

FIG. 2.—Zoom-in of the ESI spectrum of GRB 000926 on UT 2000 September 29.26 showing the existence of two components with a mean separation of ~4.05 Å at redshifts of $z_1 = 2.0370 \pm 0.0011$ (indicated by 1) and $z_2 = 2.0387 \pm 0.0011$ (indicated by 2). The spectrum has been smoothed by a boxcar of 7 pixels, equivalent to 1.12 Å.

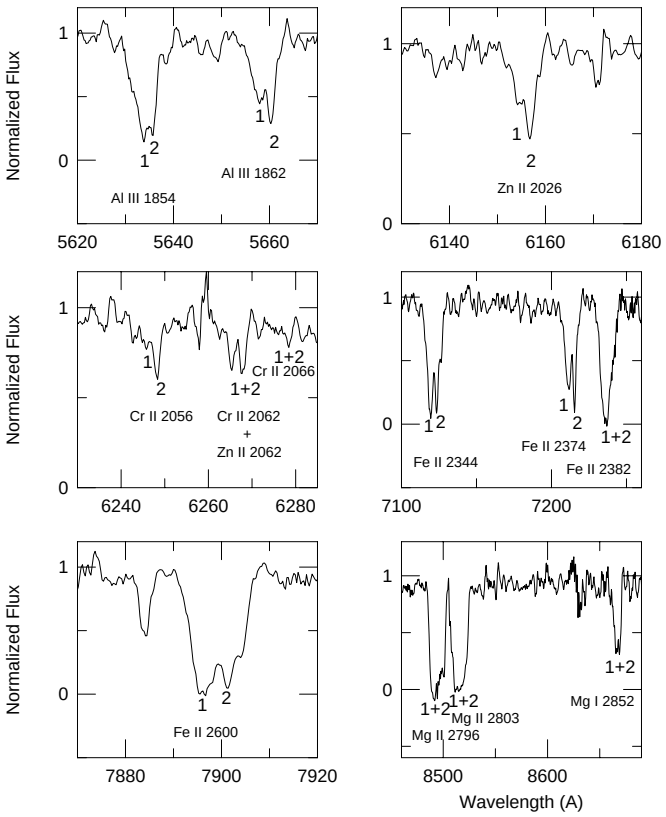

FIG. 3.—Another set of lines in the ESI spectrum, showing the two components of the absorption system.

identifications from ESI, where we list the EWs of the blended lines, since we cannot reliably separate and extract values for the components independently. We normalized the spectra with the continuum set to unity. To obtain the total EW for the blended lines, we fitted the two components separately, using the mean redshifts of the two components for extraction, which we performed using the deblend task from IRAF to fit Voigt profiles. We then added the EWs derived for the two components. The derived redshifts of the two components are $z_1 = 2.0370 \pm 0.0011$ and $z_2 = 2.0387 \pm 0.0011$, with a mean of $z = 2.0379 \pm 0.0008$. Figure 4 shows the approximate position and orientation of the ESI slit in an *HST* WFPC2 F606W image of the field. Contaminating flux from the underlying GRB host galaxy, which would cause the EWs to be underestimated, is negligible in our spectroscopic observations (see below).

Figure 5 shows the LRIS spectrum smoothed by ~3.8 Å. Table 2 shows the EWs we derived by fitting the spectrum assuming Voigt profiles for all the measured lines. The table lists both total and statistical uncertainties. The systematic errors are dominated by the uncertainty in the placement of the continuum.

A comparison of the EWs measured from the LRIS spectrum with those from the ESI spectrum (summing the two components) shows generally good agreement, apart from a small tendency for larger EWs in the LRIS spectrum. This can be entirely understood as the effect of not being able to resolve the two systems in the lower resolution LRIS data. The ESI measurements are therefore more accurate.

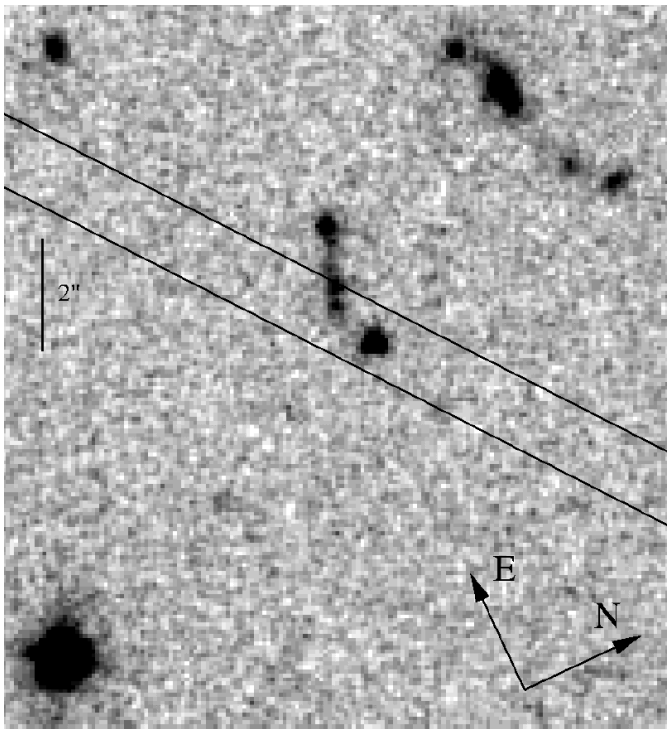

FIG. 4.—Combined *HST* WFPC2 F606W image of the GRB 000926 optical afterglow. Indicated is the approximate position and orientation of the ESI slit.

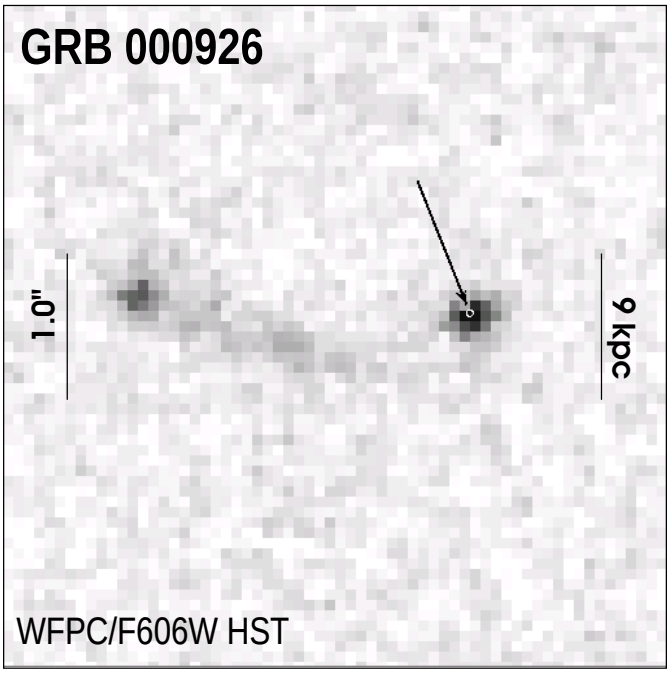

FIG. 6.—Combined *HST* WFPC2 F606W image of a $4\farcs5 \times 4\farcs5$ region surrounding GRB 000926, taken on UT 2001 May 19.72, 238 days after the event. At this epoch the emission from the GRB position is dominated by a compact and relatively bright (24.83 mag in *R*) knot. The white ellipse is the 9 σ contour position of the OT.

4. THE GRB 000926 HOST GALAXY AND OFFSET

In the final epoch *HST* images, the flux from the region is due entirely to the host galaxy. Figure 6 shows the WFPC2 F606W image from UT May 19.72 (238 days after the GRB). Table 3 provides the magnitude of the emission extracted from a $0\farcs25$ radius region surrounding the position of the OT. These magnitudes are aperture-corrected to $0\farcs5$ to match published calibrations (Holtzman et al. 1995). We then calibrated the WFPC2 data using the zero points from Holtzman et al. (1995, Table 10, p. 1086). Table 3 shows the resulting SMAGs (standard *HST* magnitude system). We then transformed to the Johnson-Cousins system using published color transformations (see Holtzman et al. 1995, Table 10). The transformed magnitudes are provided in Table 4. We note that the quoted errors are statistical only.

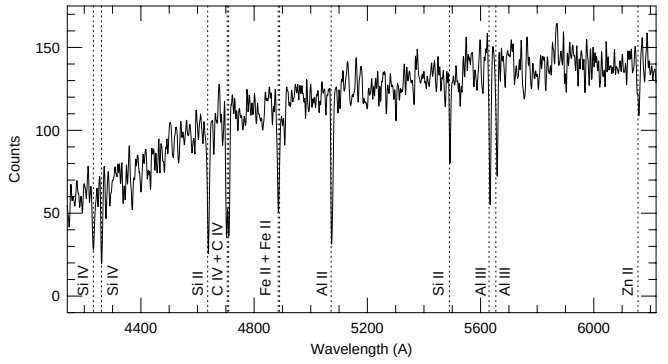

FIG. 5.—LRIS spectrum of GRB 000926 on UT 2000 September 29. Indicated are the line identifications corresponding to a redshift of $z = 2.0373 \pm 0.0011$. The spectrum has been smoothed by $\sim$3.8 Å.

To determine the extent of the knot of emission underlying the OT, we compared the radial profile to that of a standard star. Figure 7 shows the flux extracted in increasing apertures for the host emission (*diamonds*) compared to the reference star. The scale is normalized to unity for a $1''$ radius aperture. The emission is clearly extended compared to the instrument point-spread function.

To determine the precise location of the OT in the bright knot of emission, we compared the OT centroid taken from the first-epoch *HST* WFPC F606W image (when the OT emission was dominant; see Fig. 8) and compared it to the centroid of the knot seen in the late-epoch image. To register the first-epoch to the final image, we drizzled both images independently, increasing the drizzled pixel size by a factor of 2 in area (PIXFRAC = 0.8). We then registered the final stacked images from the two epochs using IRAF/CROSSCOR and IRAF/SHIFTFIND, restricting the cross-correlation to the region of overlap between the two epochs on WFPC chip 3. Using IRAF/CENTER and the OFILTER centering algorithm, we computed the centers of the OT and the knot. The result is a statistical offset of 23.9 ± 4.2 mas east, 21.2 ± 4.1 mas south (knot $\rightarrow$ OT) or $r = 31.9 \pm 4.1$ (note that the uncertainty of 4.1 mas is not

TABLE 3

HST WFPC2 OBSERVATIONS OF THE GRB 000926 HOST EMISSION IN A 2 PIXEL ($0\farcs25$) RADIUS REGION CENTERED ON THE OPTICAL TRANSIENT POSITION

Epoch	Filter	t_{obs} (s)	Magnitude
19.63	F450W	2200	25.80 ± 0.14
19.72	F606W	4400	25.47 ± 0.05
19.86	F814W	4400	24.97 ± 0.06

TABLE 4

BVRI MAGNITUDES FOR THE EMISSION EXTRACTED FROM *HST* IMAGES IN A 2 PIXEL (0″.25) RADIUS REGION CENTERED ON THE OPTICAL TRANSIENT

Band	Magnitude (2 Pixels)	Magnitude (5 Pixels)
B	25.86 ± 0.14	25.49 ± 0.33
V	25.66 ± 0.05	25.08 ± 0.06
R	25.29 ± 0.06	24.83 ± 0.07
I	24.95 ± 0.06	24.59 ± 0.01

the normal Gaussian rms; see Bloom, Kulkarni, & Djorgovski 2002 for further details). As a demonstration of the good registration of the images, we note that the bright knot of emission located 2″.57 east and 0″.15 north of the OT, which we call the eastern knot, has a statistically negligible offset of (epoch 5 → epoch 1) 11.7 ± 6.1 mas west, 8.4 ± 6.0 mas south between images. The white oval in Figure 6 shows the position of the OT compared to the bright knot.

In addition to the bright, compact knot associated with the OT, Figure 6 also shows an arc of emission extending east from the OT location, terminating in a second (eastern) knot. The arc is separated by a projected distance of ~4 kpc from the compact knot containing the OT. Ground-based narrowband Lyα imaging indicates that the extended emission also originates from $z = 2.04$ (Fynbo et al. 2002) and therefore may be associated with the host. The two bright knots, separated by ~20 kpc, are possibly the nuclei of interacting systems. We examined the colors of the eastern knot, as well as of another region (the knot in the center of the image), by extracting flux from a 5 pixel (0″.5) aperture from the summed exposures and compared to the compact knot as measured in the final epoch. For the eastern knot we derive magnitudes in the *HST* filters of $M(606) = 25.56 \pm 0.03$, $M(814) = 25.15 \pm 0.04$ and for the central knot $M(606) = 25.74 \pm 0.03$, $M(814) = 25.23 \pm 0.04$. Comparing the emission extracted from the OT position to that of the eastern knot in the F814W and F606W WFPC filters, the knot coincident with the OT appears to be somewhat redder at the 3.5 σ level.

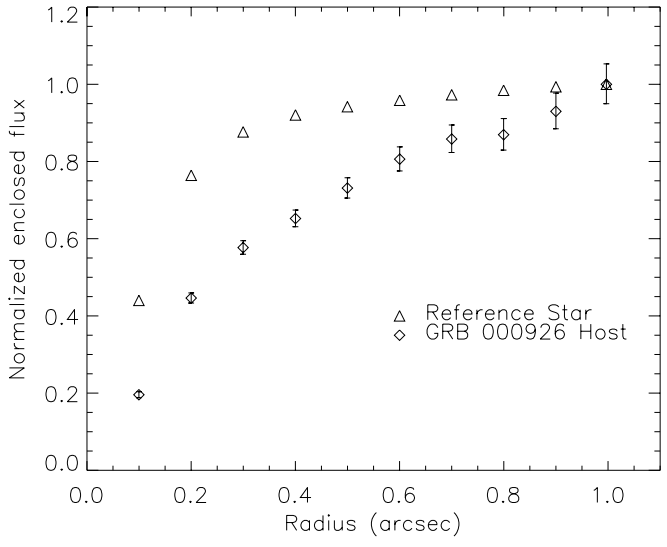

FIG. 7.—Emission from the region underlying the GRB 000926 OT as a function of extraction radius (*diamonds*) compared to a reference star (*triangles*). The vertical scale is magnitudes normalized to unity at 0″.1 radius. This clearly shows the knot of emission to be extended compared to the instrument point-spread function.

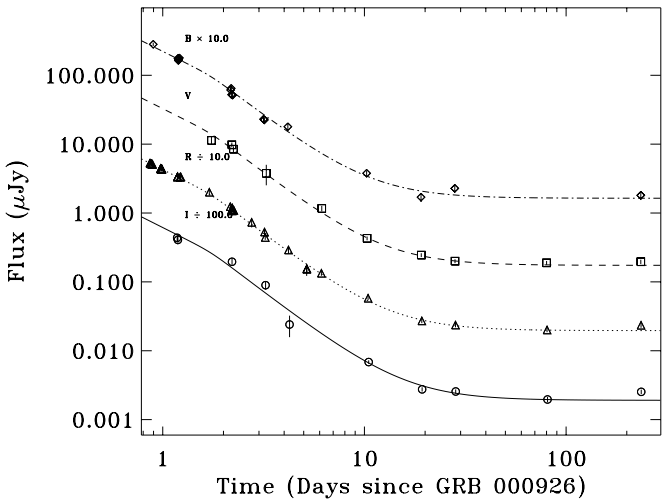

FIG. 8.—Optical light curve of GRB 000926. The data are from Price et al. (2001) and Fynbo et al. (2001) except for the last epoch, taken with *HST* WFPC2 on UT May 19.26–20.86. The lines show a model fit to the afterglow emission with a constant host contribution added.

5. DISCUSSION

Two notable features of the GRB 000926 OT are the small offset from the center of the bright knot, which we take to be the center of the host galaxy, and the large EWs of the absorption lines. At the redshift of GRB 000926, the OT offset amounts to 287 ± 37 pc projected on the sky. Only two out of 15 other GRBs have smaller measured offsets from their hosts (GRB 000418 and GRB 970508; Bloom et al. 2002). The absorption-line EWs are large compared to those seen in other GRBs. The Mg II absorption, with $W_\lambda(\text{Mg II } 2796.3) = 5.4 \pm 0.5$ Å and $W_\lambda(\text{Mg II } 2803.5) = 5.4 \pm 0.5$ Å (summing components 1 and 2), is by far the largest measured in a GRB afterglow to date. The Mg II is highly saturated; the doublet ratio $W_\lambda(\text{Mg II } 2796.3)/W_\lambda(\text{Mg II } 2803.5)$ is close to unity, compared to the factor of 2 expected for unsaturated lines. The ratio of Mg I to Mg II, $W_\lambda(\text{Mg I } 2853.0)/W_\lambda(\text{Mg II } 2796.3) = 0.45 \pm 0.06$, is also very high. In quasar absorption-line systems, this ratio is typically ≤ 0.15 (Steidel & Sargent 1992). Such a high ratio was also noted in GRB 970508 (Metzger et al. 1997).

Combined with the small offset, the high EWs indicate that the GRB 000926 OT lies close to the center of a region of high stellar density. The small offset alone means the projected distance is small, and the measured EWs imply that the line of sight subtends a significant column of material, in excess of that expected for a typical galactic halo. Damped Lyα systems are believed to be normal foreground galaxies, and the lines of sight to the back-lighting quasars most often subtend the halo of the absorber (Choudhury & Padmanabhan 2002). The Mg II features seen in damped Lyα systems at similar redshift typically have $W_\lambda(\text{Mg II } 2796.3)$ between 0 and 3 Å, falling off steeply toward high W_λ (Steidel & Sargent 1992). The sample of Steidel & Sargent (1992) contains no system with $W_\lambda(\text{Mg II } 2796.3) > 3$ Å. Our measurement of $W_\lambda(\text{Mg II } 2796.3) = 5.4 \pm 0.5$ Å is therefore exceptionally high. The large relative values that we

measure for GRB 000926 therefore imply that the OT was embedded in a dense location.

Absorption redshifts provide only lower limits; however, in this case, as argued above, the absorption is almost certainly due to the host galaxy. Assuming a $\Omega_m = 0.3$, $\Omega_\lambda = 0.7$, $H_0 = 65$ km s^{-1} Mpc^{-1} cosmology, the measured redshift and the k-corrected 20–2000 keV fluence correspond to an isotropic energy release of $(2.97 \pm 0.10) \times 10^{53}$ ergs, which reduces to 3×10^{51} ergs when corrected for collimation of the outflow (Harrison et al. 2001).

The two components seen in the ESI absorption lines are likely due to individual systems in the host galaxy. The velocity separation of 168 km s^{-1} is typical for relative motions between clouds in a galaxy. Adopting the assumption that the GRB lies in one of these clouds near the galactic center and the second cloud is at the visible half-light radius, so that the measured velocity is representative of galactic rotation at this distance, we can estimate the host galaxy mass to be $M_{\rm host} \sim v^2 r_{1/2} G^{-1} = 10^{10}\ M_\odot$.

In principle, absorption spectroscopy can be used to measure metallicity in distant galaxies, and it is interesting to ask how metal abundances in GRB hosts compare to other systems at similar redshift. Unfortunately, our spectra do not extend far enough into the blue to measure Lyα. Fynbo et al. (2001) obtained a spectrum 21.7 and 44.4 hr after the burst in which they detect a damped absorption line due to neutral hydrogen. From the line, they infer an H I column of 2×10^{21} cm^{-2}. We use this measurement, combined with the EW from our ESI spectrum in Table 5, for those lines that do not suffer severe saturation.

The relative abundances of various metals can be used to make some inferences about the physical properties of the absorbing medium. For example, the relative abundances of zinc and chromium, as measured from the Zn II ($\lambda\lambda$2026.15, 2062.66) and Cr II ($\lambda\lambda$2056.25, 2062.23, 2066.16) lines provide a qualitative estimate of the dust-to-gas ratio in the absorbing clouds. In a study of these lines in damped Lyα systems, Pettini et al. (1990) noted that the Zn II doublet provides a good measurement of Zn in the gas phase of the ISM and, further, that Zn is not readily incorporated into dust grains. Interstellar Cr, on the other hand, is one of the most heavily depleted elements (see Pettini et al. 1990 for more detailed discussion).

We detect Zn II λ2026 and Cr II λ2056 with high statistical significance in a region of the spectrum where we can accurately measure the continuum, and these EWs are listed in Table 1. We cannot resolve the Cr II λ2062.23 and Zn II λ2062.66 lines, but we measure the combined redshift-corrected EW of $W = 0.23 \pm 0.02$ (0.01) Å ($z = 2.03927$) and $W = 0.05 \pm 0.01$ (0.01) Å ($z = 2.03885$) for the blend. The Cr II λ2066 line is only marginally detected, and the EW is difficult to extract since the line lies in a region where it is very difficult to measure the continuum. Based on upper and lower limits on the continuum, we estimate 0.18 Å $> W >$ 0.09 Å ($z = 2.03874$). From the total zinc column, we infer that the Zn II and Cr II lines are not heavily saturated, and we can therefore use the EWs to estimate the relative abundances of Zn and Cr. This is confirmed by Savaglio, Fall, & Fiore (2002), who use a curve-of-growth analysis to derive columns for these lines that are within 10% of the values in Table 5.

The Cr/Zn ratio that we measure for the absorbers in the GRB 000926 host indicates that the host galaxy is depleted in dust relative to the local ISM. The ratio [Cr/Zn] for both components of the absorption system is significantly larger than that measured locally. Using the oscillator strengths from Pettini et al. (1994), we obtain $[{\rm Cr/Zn}] = -0.55 \pm 0.09$, indicating the gas-phase abundance of Cr is almost a factor of 10 higher than in the local ISM. [Cr/Zn] measured for the GRB 000926 clouds is in fact quite similar to the range Pettini et al. (1994) obtain for damped Lyα systems between $2 < z < 3$. For the damped Lyα systems, Pettini et al. (1994) concluded that this is due to the depletion of dust in high-redshift galaxies. A similar qualitative statement applies to the GRB 000926 host, again assuming that the absorption systems are local to the host.

6. CONCLUSIONS

High-resolution absorption spectroscopy of GRB 000926 strengthens the case that GRBs explode in dense locations. The small offset from the center of the bright, compact knot—likely the nucleus of the host galaxy—combined with the evidence for a significant column depth of metals indicates the explosion occurred in a dense central region of a galaxy at redshift $z = 2.038$. The two absorption systems seen in the intermediate-resolution spectra, separated by $v = 168$ km s^{-1}, are most easily interpreted as due to separate clouds within the host galaxy.

The ability to measure the EWs of a significant number of metal lines in the GRB 000926 spectrum suggests that in the future, high-resolution studies of OTs will provide a means of probing the metallicity and dust content of GRB hosts. From the ratio Cr/Zn, it appears that, like other galaxies at similar redshift, the dust-to-gas ratio is reduced in the GRB 000926 host compared to local values. With a larger sample of GRB transients with high-quality absorption spectroscopy, it will be possible in the future to compare the enrichment of GRB hosts to damped Lyα systems in a statistically meaningful way and to determine if there are any significant differences in metal enrichment and dust depletion relative to other distant galaxies.

The spectra presented in this paper were obtained at the W. M. Keck Observatory, which is operated as a scientific partnership among the California Institute of Technology,

TABLE 5
METAL COLUMNS AND ABUNDANCES FOR THE ABSORPTION SYSTEM MEASURED BY ESI

Line	f	$\log[N({\rm X})]$	$\log[N({\rm X})/N({\rm H})]$	$\log[N({\rm X})/N({\rm H})]_\odot$
Fe II λ1608.46.....	0.058	15.21	−6.09	−4.49
Si II λ1808.00.....	0.00218	16.25	−5.05	−4.45
Zn II λ2026.14	0.489	13.70	−7.60	−7.35
Cr II λ2056.25.....	0.105	14.25	−7.05	−6.32
Fe II λ2374.46.....	0.0313	15.22	−6.08	−4.49

the University of California, and the National Aeronautics and Space Administration. The Observatory was made possible by the generous financial support of the W. M. Keck Foundation. We want to thank the staff of the W. M. Keck Observatory for their valuable assistance. We are grateful to L. Cowie and R. Ellis for taking the spectra at the time needed. We thank J. U. Fynbo for his constructive comments, which helped us improve the discussion presented in this paper.

This work was supported by NSF and NASA (under contract NAS5-26555). S. R. K. and S. G. D. are supported in part by NSF and NASA. T. J. G. thanks the Fairchild Foundation, and F. A. H. acknowledges support from a Presidential Early Career award.

REFERENCES

Bloom, J. S., Djorgovski, S. G., & Kulkarni, S. R. 2001, ApJ, 554, 678
Bloom, J. S., Kulkarni, S. R., & Djorgovski, S. G. 2002, AJ, 123, 1111
Castro, S., Djorgovski, S. G., Kulkarni, S. R., Bloom, J. S., Galama, T. J., Harrison, F. A., & Frail, D. A. 2000, GCN Circ. 851 (http://gcn.gsfc.nasa.gov/gcn/gcn3/851.gcn3)
Choudhury, T. R., & Padmanabhan, T. 2002, ApJ, 574, 59
Dall, T., Fynbo, J. P. U., Pedersen, H., Jensen, B. L., Hjorth, J., & Gorosabel, J. 2000, GCN Circ. 804 (http://gcn.gsfc.nasa.gov/gcn/gcn3/804.gcn3)
Djorgovski, S. G., Frail, D. A., Kulkarni, S. R., Bloom, J. S., Odewahn, S. C., & Diercks, A. 2001, ApJ, 562, 654
Epps, H. W., & Miller, J. S. 1998, Proc. SPIE, 3355, 48
Fruchter, A., Krolik, J., & Rhoads, J. 2001, ApJ, 563, 597
Fruchter, A. S., & Hook, R. N. 2002, PASP, 114, 144
Fynbo, J. P. U., Møller, P., Dall, T., Pedersen, H., Jensen, B. L., Hjorth, J., & Gorosabel, J. 2000, GCN Circ. 807 (http://gcn.gsfc.nasa.gov/gcn/gcn3/807.gcn3)
Fynbo, J. P. U., et al. 2001, A&A, 373, 796
———. 2002, A&A, 388, 425
Gorosabel, J., Castro Cerón, J. M., Castro-Tirado, A. J., Greiner, J., Wolf, C., & Lund, N. 2000, GCN Circ. 803 (http://gcn.gsfc.nasa.gov/gcn/gcn3/803.gcn3)
Groot, P. J., et al. 1997, IAU Circ. 6574
Harrison, F. A., et al. 2001, ApJ, 559, 123
Holtzman, J. A., Burrows, C. J., Casertano, S., Hester, J. J., Trauger, J. T., Watson, A. M., & Worthey, G. 1995, PASP, 107, 1065
Hurley, K., Mazets, E., Golenetskii, S., & Cline, T. 2000, GCN Circ. 801 (http://gcn.gsfc.nasa.gov/gcn/gcn3/801.gcn3)
MacFadyen, A. I., & Woosley, S. E. 1999, ApJ, 524, 262
Metzger, M. R., Djorgovski, S. G., Kulkarni, S. R., Steidel, C. C., Adelberger, K. L., Frail, D. A., Costa, E., & Fronterra, F. 1997, Nature, 387, 879
Oke, J. B., et al. 1995, PASP, 107, 375
Perna, R., & Loeb, A. 1998, ApJ, 501, 467
Pettini, M., Boksenberg, A., & Hunstead, R. W. 1990, ApJ, 348, 48
Pettini, M., Smith, L. J., Hunstead, R. W., & King, D. L. 1994, ApJ, 426, 79
Price, P. A., et al. 2001, ApJ, 549, L7
Savaglio, S., Fall, S. M., & Fiore, F. 2002, ApJ, submitted (astro-ph/0203154)
Steidel, C. C., & Sargent, W. L. W. 1992, ApJS, 80, 1
Taylor, G. B., Frail, D. A., Kulkarni, S. R., Shepherd, D. S., Feroci, M., & Frontera, F. 1998, ApJ, 502, L115
Waxman, E., & Draine, B. T. 2000, ApJ, 537, 796